

Class3Dp: A supervised classifier of vegetation species from point clouds

Juan Pedro Carbonell-Rivera ^{*}, Javier Estornell, Luis Ángel Ruiz, Pablo Crespo-Peremach, Jaime Almonacid-Caballer, Jesús Torralba

Geo-Environmental Cartography and Remote Sensing Group (CGAT), Universitat Politècnica de València, Camí de Vera s/n, 46022, València, Spain



ARTICLE INFO

Keywords:

Species classification
Bare-earth extraction
Machine learning
Coloured point cloud
Unmanned aerial vehicles (UAV)
Digital aerial
Photogrammetry (DAP)

ABSTRACT

Recognizing the species composition of an ecosystem is essential for conservation and land management. This study presents the software Class3Dp, a supervised classifier of vegetation species for coloured point clouds. Class3Dp is run through a graphical user interface (GUI) that allows for the selection of training samples from RGB or MS (multispectral) clouds and their classification based on geometric, spectral and neighbourhood features, along with different machine learning methods, obtaining the point cloud classified according to the classes (species) introduced. A case study is shown where a classification of ground and vegetation is carried out, obtaining an overall accuracy (OA) of 0.94 in the RGB classification and 0.95 in the MS. Points classified as vegetation were re-classified in the species *Anthyllis cytisoides* L., *Chamaerops humilis* L., *Cistus monspeliensis* L., *Pistacia lentiscus* L. and *Quercus coccifera* L., obtaining an OA of 0.86 in the RGB classification and 0.87 in the MS.

Software and data availability

- Software name: Class3Dp.
- Developers: Juan Pedro Carbonell-Rivera, Javier Estornell Cremares, Luis Ángel Ruiz Fernández.
- First year available: 2023.
- Hardware requirements: PC.
- Program language: Python.
- Access to the compressed file with source code, executable file and tutorial of use available: <http://hdl.handle.net/10251/193787>
- License: GNU GPL v3.0
- Program size: 638 MB
- Access to the compressed file with the dataset from the case study: <https://doi.org/10.4995/Dataset/10251/194199>
- Dataset license: CC BY-NC-SA 4.0
- Dataset size: 206 MB

1. Introduction

The ability to locate and identify plants allows the assessment of ecosystem variables that are critical for proper management, such as species richness and species evenness (Hooper and Vitousek, 1997). The location of individual plants classified by species contributes to determine the health and dynamics of an ecosystem. In addition, applications

in conservation and sustainable forest management, such as biodiversity monitoring, climate change studies, forest inventories, risk management or wildlife habitat modelling, rely significantly on the classification of plant species (Diaz et al., 2000).

The classification of plant species has traditionally been addressed using remote sensing (RS), based on spectral and geometric differences (Al-doski et al., 2013). RS imagery, especially space-borne imagery, has been widely used to classify vegetation communities and, to discriminate forest types and tree species at different spatial and spectral levels: low-spatial and medium-spectral resolution MODIS imagery (Ivanova et al., 2019); medium-spatial and high-spectral resolution PRISMA imagery (Vangi et al., 2021); medium-spatial and medium-spectral resolution Landsat or Sentinel imagery (Wang et al., 2018), and high-spatial and medium-spectral resolution WorldView imagery (Ferreira et al., 2019). However, these images, even those with high-spatial resolution such as WorldView images (0.31 m using pansharpening techniques), cannot discern the composition of small herbaceous or shrub species, which are usually mixed (Carbonell-Rivera et al., 2022; Lu and He, 2017).

In recent years, UAVs have emerged as an alternative to the use of aircraft or satellite platforms for geospatial data acquisition (Meinen and Robinson, 2021). UAVs allow for the acquisition of very high spatial resolution images due to their low altitude operation, which makes these systems less constrained by atmospheric conditions. Compared to

* Corresponding author.

E-mail address: juacarri@upv.es (J.P. Carbonell-Rivera).

manned aircrafts, UAVs reduce the cost of acquisition, maintenance and operation, as well as the complexity of data collection. The application of photogrammetry and Structure from Motion (SfM) algorithms allows to obtain products such as point clouds, 3D objects, or orthophotos using only a consumer camera (Ullman, 1979). In this context, UAV systems can carry different sensors such as RGB digital cameras, multispectral (MS) or hyperspectral sensors, or light detection and ranging (LiDAR) sensors. The information extracted from UAV-based digital aerial photogrammetry (UAV-DAP) allows for pixel-based and point-based classifications. Point-based classifications have the advantage of using 3D information obtained from the point cloud (Gao et al., 2022; Marselis et al., 2016). These point data, in addition to geometric information, contain spectral information associated with the photogrammetric process and the matched parent pixel from the raw image (Iglhaut et al., 2019; Wallace et al., 2016). The addition of spectral information in point clouds is not unique to UAV-DAP, as those obtained from laser instrumentation may also contain spectral information if one or more images are projected onto the point cloud (Leberl et al., 2010). However, the delay between the image and the laser shot can lead to registration errors due to changes in the environment or poor calibration between the LiDAR sensor and the camera (González et al., 2022). For this reason, applications of this combination of spatial and spectral information in a single data source have been focused on the use of UAV-DAP point clouds (Carbonell-Rivera et al., 2022; Mesas-Carrascosa et al., 2020; Nevalainen et al., 2017).

Point-based classification in RS, as well as image classification, is commonly divided into two methods: supervised and unsupervised classification (Ripley, 1996; Sathya and Abraham, 2013). Supervised classification involves the use of algorithms to classify data points and objects into different categories, using existing labelled data as a reference (Sathya and Abraham, 2013). In supervised classification, data points are labelled into predefined classes. In contrast, unsupervised classification involves the use of algorithms to assign data points or objects to groups without having any predefined labels (Ripley, 1996; Sathya and Abraham, 2013). This method is based on analysing data and finding patterns and similarities between different objects, without the use of predefined classes for classification. Supervised classification is widely used as a statistical approach for vegetation classification based on the similarity of species composition (Atik et al., 2021; Cabo et al., 2019; Deng et al., 2022; Mesas-Carrascosa et al., 2020; Molina-Valero et al., 2022; Nevalainen et al., 2017; Sothe et al., 2019).

Traditionally, point-based classification has been developed specifically for LiDAR point clouds. In this sense, point cloud classification software have traditionally relied solely on geometric information. This type of software is capable of classifying UAV-DAP point clouds, using only geometric information without considering spectral information. Currently, the lack of specific software to handle UAV-DAP point clouds is limiting its potential (Yancho et al., 2019). Software such as LASStools (Isenburg, 2014) or Fusion/LDV (McGaughey, 2016) use geometrical algorithms to classify bare ground points. Others, such as Agisoft Metashape (Agisoft LLC., 2022) or Pix4d, have integrated unsupervised classification methods for the classification of point clouds according to different predefined generic classes, not allowing the user to define new classes. The possibility to perform supervised classifications on photogrammetric point clouds based on their geometric and spectral properties would allow their application in a wide range of fields. In 2022, Carbonell-Rivera et al. showed a methodology for classifying vegetation species by combining spectral and geometrical features from multispectral point clouds. In this study, mean cross-validation accuracies of 81.7% and 91.5% were achieved in two test sites encompassing a study area of 14,344 m². Consequently, this prompted the proposal for the development of a user-friendly point cloud classification software, enabling users to classify point clouds with ease, even without prior programming expertise.

This study proposes a new software tool, Class3Dp, to apply a supervised classification to point clouds using point spatial distribution

and spectral information. With Class3Dp, a user can process large datasets of points to identify and classify tree and shrub species in a given area. A classified point cloud with flora data can provide accurate information on species, height and density, which can help ecologists and resource managers make decisions about ecosystem management, including identifying priority conservation areas and planning forest restoration activities. In addition, these classified point clouds can be used to analyse the richness and composition of tree and shrub species, key information for evaluation and management of ecosystems.

2. Software description

The open source software Class3Dp (Carbonell Rivera et al., 2023a) allows the supervised classification of point clouds using 3D and spectral information. This software is operated through a graphical user interface (GUI), enabling the selection of samples and the extraction of different geometric, spectral and neighbourhood features to train different machine learning models selected by the user. Fig. 1 shows the typical workflow of a classification process using Class3Dp.

The software is divided into two modules. The first one is focused on the selection of training samples, and the second one on the rest of the classification process, either using RGB or MS data. In this paper, the point cloud containing red, green and blue bands will be referred as RGB point cloud, while the one with the bands blue, green, red, red-edge and near-infrared will be referred as MS point cloud.

2.1. Point cloud sampling

For the selection of training and validation samples, Class3Dp allows the three-dimensional visualization of RGB and MS point clouds (Fig. 2). The input file format for the RGB point cloud is LAS (.las), while for the MS point cloud it is a space separated ASCII format (.txt) with the information: X, Y, Z, blue, green, red, red-edge, NIR.

In the case of MS point clouds, the user can select the bands to be displayed, allowing the creation of false colour composites to facilitate the selection of samples. The software supports MS point clouds created from imagery with five bands: blue, green, red, red-edge and near-infrared. These bands correspond to the most commonly used multispectral cameras available on the market. Once the point cloud is loaded, the user can select samples and the points selected for each class will be saved separately in different files. In this sense, the user can enter in Class3Dp training samples created in other programs, following the aforementioned formats.

2.2. Feature extraction

In order to perform the classification of point clouds, the software is able to calculate up to 48 different features per point to potentially be introduced in the model (Table A1). These features are generated from the geometric information of the points (X, Y, Z coordinates) and the spectral information (green, blue, red, red-edge or near-infrared bands), and they are divided into different types: geometrical, spectral and neighbourhood-based including geometrical and spectral. The neighbourhood of a point is defined as $p \in R^3$, R^3 being the set of points inside a sphere s , of centre p , and radius defined by the user. From the coordinates (X, Y, Z) of each point, 17 geometric features are generated based on the neighbourhood of each point. These features are based on the average and standard deviation distance of the points in the neighbourhood (Dist_mean and Dist_std), and on the height differences in the neighbourhood (Z_mean, Z_std, Dif_Z, Z_min, Z_max-Z and Verticality). By analysing the geometry within a defined neighbourhood around each point of the cloud, different vegetation species can be distinguished, considering the geometric characteristics of each plant species. The covariance matrix of a point cloud neighbourhood provides information about the distribution and orientation of the points in the neighbourhood around a given point. The eigenvalues of the covariance matrix

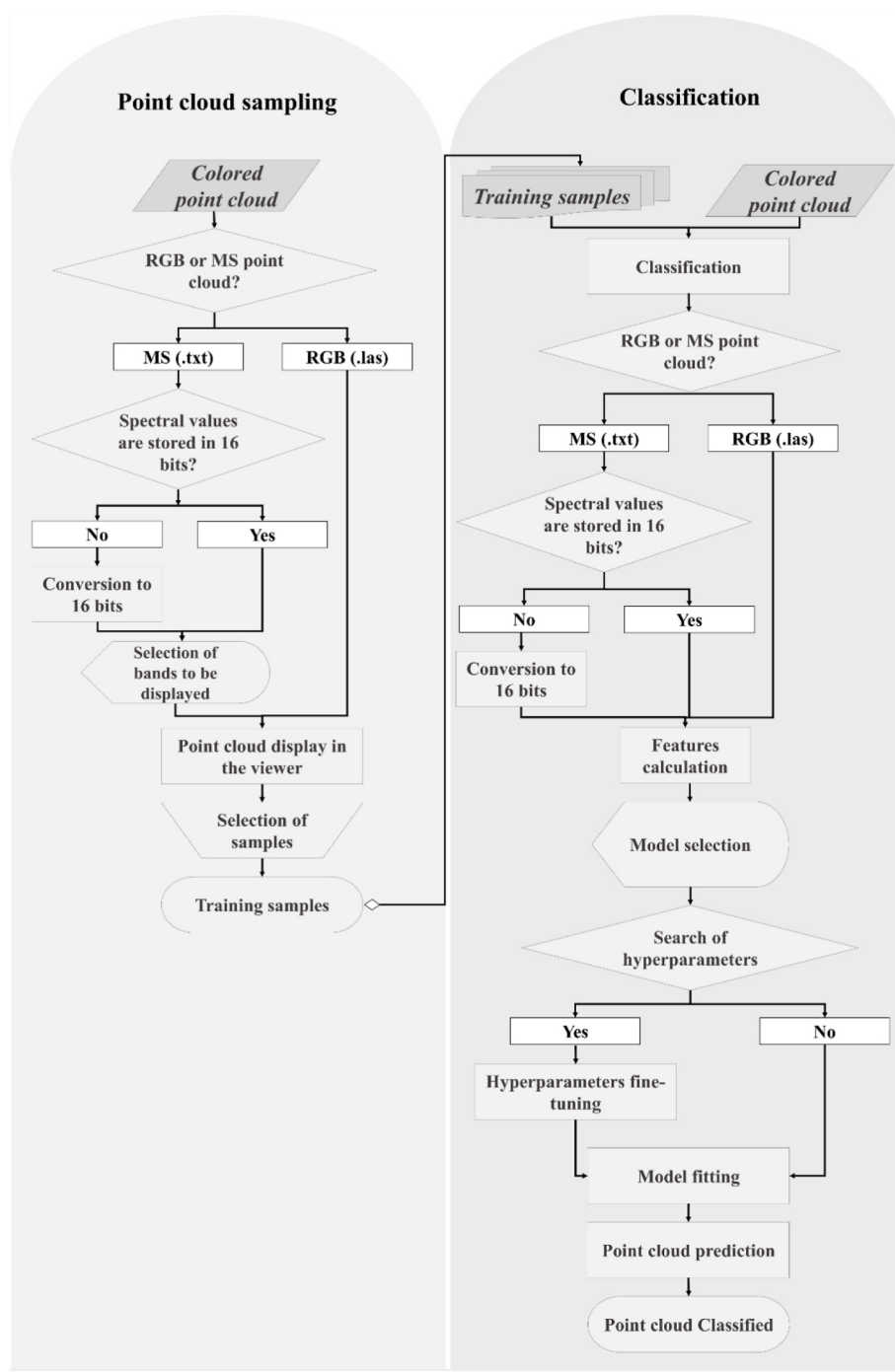


Fig. 1. Point cloud classification workflow of Class3Dp.

correspond to the principal axes of the distribution, encoding the variability of the data on an orthogonal basis (Sum $_{\lambda}$, Omnivariance, Eigenentropy, Anisotropy, Planarity, Linearity, Surface Variation and Sphericity).

Vegetation types and species have different structural characteristics that influence the distribution and orientation of the points in their point clouds. For example, a tall and dense forest canopy may have a more elongated and uniform distribution of points compared to a patch of low-lying shrubs, which may have a more irregular and clustered distribution of points. By summing the eigenvalues of the covariance matrix for each neighbourhood in a point cloud (feature Sum $_{\lambda}$), a global measure of the point distribution is captured (Rusu, 2009). The omnivariance measures the variance of the point covariance matrix

eigenvalues in the neighbourhood of a given point (West et al., 2004). It is useful for capturing the overall shape and orientation of the vegetation. The eigenentropy measures the entropy of the point covariance matrix eigenvalues in the neighbourhood of a given point (West et al., 2004). It captures the level of disorder or randomness in the shape of the vegetation. The anisotropy measures the difference between the largest and smallest eigenvalues (West et al., 2004), and it captures the level of elongation or stretching in the vegetation. The planarity measures the extent to which the points in the neighbourhood of a given point lie in a planar surface (West et al., 2004). It can be used to distinguish between vegetation with a flat form and that with a curved form. The linearity measures the extent to which the points in the neighbourhood of a given point lie in a straight line (West et al., 2004). It can be used to distinguish



Fig. 2. Sample selection window with the Class3Dp software. The yellow square represents the selection of a ground class sample.

between vegetation with straight branches and with curved branches. The surface variation measures the variability of the surface of the grid composed of the neighbourhood of points (Rusu, 2009). It captures the level of variation in the surface of the vegetation. The sphericity measures the degree of similarity of the neighbourhood of points with respect to a spherical surface (West et al., 2004). It can be used to distinguish between vegetation with spherical shapes and those with elongated shapes. Finally, the verticality describes the orientation of the neighbourhood of points with respect to the vertical reference axis (Demantké et al., 2012). These features can be obtained from both RGB and MS point clouds, as they are independent of the spectral information.

The program also enables computing 27 vegetation indices: ARVI (Kaufman and Tanre, 1992), BI (Fraser et al., 2017), CIVE (Kataoka et al., 2003), DVI (Richardson and Wiegand, 1977), EVI (Huete et al., 1999), GLI (Dong, 2014), GNDVI (Gitelson et al., 1996), GR (Fraser et al., 2017), IPVI (Ray et al., 1993), MGVGRI (Barbosa et al., 2019), MSAVI (Qi et al., 1994), MSR (Chen, 1996), NBRDI (Carbonell-Rivera et al., 2020), NVDI (Rouse et al., 1974), NGBDI (Shimada et al., 2012), NGRDI (Hunt et al., 2005), NormG (Stricker et al., 2014), OSAVI (Rondeaux et al., 1996), RDVI (Roujean and Breon, 1995), RGRI (Gamon and Surfus, 1999), RVI (Jordan, 1969), SAVI (Huete, 1988), SARVI (Huete, 1988), SR (Tucker, 1979), SRxNDVI (Gong et al., 2003), VARI (Gitelson et al., 2002) and vNDVI (Costa et al., 2020); see table A1 for full names. Spectral indices enhance the information content of remote sensing data. They can provide additional information about the properties of vegetation or other land cover classes that are not easily discernible from raw data. Depending on whether the point cloud is RGB or MS, different spectral indices can be obtained. For instance, the NDVI, which uses the infrared band, is only available for MS point cloud classification. In contrast, other indices, such as NBRDI, which only uses the red and blue bands, are available for both RGB and MS classifications. Additionally, Class3Dp allows obtaining four neighbourhood spectral features (NDVI_mean, NDVI_std, NGRDI_mean and NGRDI_std). Spectral indices such as NDVI are commonly used to measure vegetation health (Rouse et al., 1974); other indices such as EVI are used to detect changes in vegetation cover density and canopy structure (Huete et al., 1999). SAVI is similar to EVI, but it is adjusted to account for soil reflectance, making it more suitable for areas with varying soil properties (Huete, 1988). The MSAVI is similar to SAVI, but designed to minimize the effect of soil reflectance on vegetation index values, which is used to distinguish between vegetation and bare soil, and to estimate LAI in areas with varying soil reflectance (Qi et al., 1994). Other indices, such as the Green Leaf Index (GLI), Green-Red Vegetation Index (GRVI), and Red-Edge Chlorophyll Index (CRed-edge), are designed to specifically target certain vegetation properties, such as leaf area or chlorophyll content. These indices can be particularly useful for characterizing different plant species or detecting stress in vegetation. In general, RGB or MS bands, together with vegetation indices provide information to

the classifier by enhancing the contribution of vegetation properties and allowing the distinction of spectral properties inherent to each species.

2.3. Classification algorithms

After the input feature selection, the user should select the classification method. Class3Dp enables the selection of the following machine learning methods: Decision Tree (Pedregosa et al., 2011), Extra Trees (Geurts et al., 2006), Gradient Boosting (Friedman, 2001), Random Forest (Breiman, 2001) and the MultiLayer Perceptron (Hinton, 1990). The software allows users to select a specific classification method or perform an automatic process that runs all the methods and selects the one that obtains the highest mean cross-validated score (mCVs) (Ojala and Garriga, 2010) with 10 folds to ensure the independence between training and test data. For the evaluation of these methods, a fine-tuning of the hyperparameters can be done to optimize the models. This fine-tuning is carried out by setting up a grid of hyperparameters (Table 1). If the user chooses not to perform this fine-tuning, the default hyperparameters for Decision Tree, Extra Trees and Gradient Boosting will be: Maximum depth of the tree is parameterized to None; Minimum number of samples required to split an internal node is parameterized to 2; Minimum number of samples required to be at a leaf node is parameterized to 1. The maximum depth of a decision tree determines the maximum number of levels in the tree. This hyperparameter limits the complexity of the decision tree, preventing it from becoming too deep and overfitting the training data. The minimum number of samples required to split an internal node is a hyperparameter that determines the minimum number of data points required at a node before it can be split further. This hyperparameter prevents the tree from splitting on noisy or irrelevant features by ensuring that the node has enough data points to provide reliable statistics. Finally, Minimum number of samples required to be at a leaf node controls the tree's ability to generalize to new data by limiting the number of samples at a leaf node. If this value is set too low, the tree may create leaves with very few samples, which can result in overfitting. On the other hand, if the value is set too high, the tree may be too general and not capture enough details in the data.

The default hyperparameters for Random Forest are: Number of trees in the forest, 100; the Number of features to consider is set to sqrt; the Maximum depth of the tree is parameterized to None; the function to measure the quality of a split is set to Gini. The number of trees determines the number of decision trees that will be trained during the

Table 1
Hyperparameters used for fine-tuning the models.

	Decision Tree, Extra Trees and Gradient Boosting	Random Forest	MultiLayer Perceptron
Hyperparameter #1 (values)	Maximum depth of the tree (5, 10, None)	Number of trees in the forest (100–500)	Number of neurons in the ith hidden layer (50,50,50), (50,100,50), (100)
Hyperparameter #2 (values)	Minimum number of samples required to split an internal node (2, 3, 5)	Number of features to consider ('auto', 'sqrt', 'log2')	Activation (Tanh, 'ReLU')
Hyperparameter #3 (values)	Minimum number of samples required to be at a leaf node (1, 2, 5)	Maximum depth of the tree (4, 5, 6, 7, 8)	Optimizer (SGD, Adam)
Hyperparameter #4 (values)	–	Function to measure the quality of a split ('Gini', 'entropy')	Learning rate (0.0001, 0.05)

model building process. Increasing the number of trees in the forest generally leads to better performance on the test data, but at the cost of increased computational resources required to train and evaluate the model. The number of features parameter is important for controlling the complexity of the decision tree. Including too many features may lead to overfitting, while including too few may lead to underfitting. The function used to measure the quality of a split is a hyperparameter that determines how the decision tree algorithm selects the best feature to split on at each node. The choice of the function can impact the performance of the model and the optimal function depends on the characteristics of the dataset and the problem to be solved.

For the MultiLayer perceptron algorithm, the default parameters are Number of neurons in the i th hidden layer, which is set to 100; Rectified Linear Activation (ReLU) (Nair and Hinton, 2010) is used as activation function; Adaptive Moment Estimation (Adam) (Kingma and Ba, 2014) is parameterized as Optimizer; the Learning rate default value is 0.0001. The number of neurons determines the number of nodes or neurons in the i th hidden layer of an artificial neural network. The number of neurons can affect the complexity and capacity of the model, which can impact the model's ability to learn and generalize from the training data. For the optimal activation, the function set depends on the problem to be solved, the architecture of the network, and the dataset to be used. Different activation functions can impact the performance of the model in terms of accuracy, training time, and generalization. The Optimizer is a hyperparameter that determines the algorithm used to update the weights and biases of the model during the training. The choice of the Optimizer can impact the speed and stability of the training process, as well as the quality of the final model. Finally, the learning rate determines the step size used to update the weights and biases of the model during training. A high learning rate can accelerate convergence but also reduce performance. A low learning rate can result in more stable training and better generalization but may require more iterations to converge on the optimal weights.

The accuracy of each combination of hyperparameters is assessed by 10-fold cross-validation to ensure the independence between training and test data. In the model fine-tuning option, the hyperparameters applied for each method are those with the highest mCVs. After model fitting, the mean and standard deviation values of the results obtained in the 10 cross-validation iterations are displayed. Then, the feature importance indicators (Breiman, 2001) are computed for each feature, allowing the user to re-evaluate the model using only the most relevant

features for each specific problem. The software allows both, to save and to load the processed models, permitting the generated classification models to be applied to other point clouds. At the end of the process, the result of the classification is stored in the "Classification" field in the case of ".las" files, or in the last column of scalar fields in the case of ".txt" files.

3. Case application of Class3Dp

In order to show the application of the UAV-DAP point cloud classification process and methods of Class3Dp, this section describes a case study in two phases. First, it is used for the classification of bare-ground points for height normalization. Subsequently, Class3Dp is used for the classification of plant species at point level.

The data for this case study is from an area located in the natural park of Sierra Calderona, specifically in the municipality of Gilet (Valencia, Spain). The Sierra Calderona natural park is one of the most valuable landscapes of the region since its natural and physical characteristics make it of great environmental, scenic, and cultural value. A circular area encompassing 1000 m² was selected (Fig. 3). The shrub density is very high, forming an almost continuous horizontal layer of vegetation, where the different species are mixed without reaching a height of more than 150 cm. Individuals from *Anthyllis cytisoides* (Albaida), *Chamaerops humilis* (European fan palm), *Cistus monspeliensis* (Montpelier cistus), *Pistacia lentiscus* (Mastic) and *Quercus coccifera* (Kermes oak) are located in the area.

Field data collection took place on July 23, 2020. The field campaign was divided into two phases: in the first, optical data was collected using UAV; in the second, individuals of the different species were located using a Global Navigation Satellite System (GNSS) receiver. UAV field-work consisted of two flights: one flight carried an RGB sensor (DJI Zenmuse X5S) and the other an MS sensor (Micasense RedEdge). Following the flights, GNSS data was collected to locate the most representative shrub species in the area. In this task, the projection on the floor of the centre of 83 individuals was measured using a GNSS receiver.

3.1. Class3Dp applied to bare-ground points classification

From the UAV images, photogrammetric Structure from Motion (SfM) algorithms were applied to obtain the RGB and MS point clouds

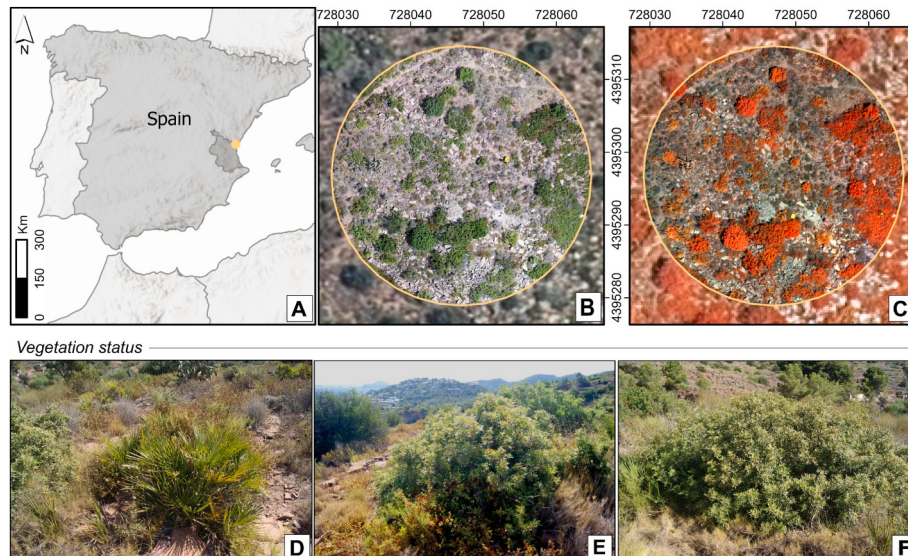


Fig. 3. Study area location in the central Mediterranean area of Spain (A). Study area RGB orthomosaic generated from UAV imagery (B). Orthomosaic in false colour infrared (C). Map reference system is EPSG:25830, coordinates in meters. Detail ground photographs of *Chamaerops humilis* (D) and *Pistacia lentiscus* (E and F) in the study area.

(Agisoft LLC., 2022), being this dataset distributed under open source license (Carbonell Rivera et al., 2023b). These point clouds were entered as input data into Class3Dp to classify bare-ground points in a first stage. To this end, the software was used to select training samples on the colour point cloud where the ground points can clearly be distinguished (Fig. 2). Once the training samples were taken, the clouds were classified in two phases: (i) ground and vegetation classification; and (ii) species classification. In the first phase, all the features calculated by the software were used, except the features X, Y, Z, Z_mean, Dif_Z, Z_Zmin and Zmax_Z, as these variables are not related to the distinction between ground and vegetation points. Once the first classification was performed, a new classification was performed, selecting only the features with the highest importance and performing a dimensional reduction. After the classification of bare-ground and vegetation points, an external software may be used (e.g., LASStools) to construct a ground Triangulated Irregular Network (TIN) using the points classified as bare ground (Isenburg, 2014). Then, the difference in height between vegetation points and the generated bare ground TIN was calculated, assigning this height to the Z coordinate of each vegetation point, obtaining the normalized point cloud. After height normalization, the points of the UAV-DAP cloud classified as bare ground and with a height below zero were omitted.

3.2. Classification of vegetation species

After the normalization process, classification of the species in the study area (*Anthyllis cytisoides*, *Chamaerops humilis*, *Cistus monspeliensis*, *Pistacia lentiscus* and *Quercus coccifera*) was applied. In this case, the samples were extracted from the GNSS points collected in the field, registering the location of the different species individuals. A 40-cm buffer was made at each point using the functions lasboundary and lasclip of LASStools. This value was selected considering the minimum radius of the smallest individuals identified. The point cloud was clipped using this radius to obtain the training samples. After this step, two classifications were performed with Class3Dp, using both RGB and MS information. In this last case, all the features allowed by the software were computed, except for the X and Y coordinates, since the geographical distribution of the species is not relevant at this scale. Both classifications were parameterized to select the best classification model automatically, calculating the best hyperparameters of each classifier.

3.3. Evaluation

Finally, an external validation of the vegetation species classification was performed by taking independent samples interpreting the point cloud. Validation samples were taken using Class3Dp (section Point cloud sampling) and were the same for RGB and MS clouds. The validation samples were compared with the predictions obtained by the Class3Dp software using a confusion matrix (Congalton et al., 1981). The precision (Pr) (Cleverdon and Keen, 1966), recall (Re) (Cleverdon and Keen, 1966), and F-measure (Fm) (Van Rijsbergen, 1979) values were also obtained using the following equations:

$$A = \begin{bmatrix} a_{1,1} & a_{1,2} & \dots & a_{1,j} \\ a_{2,1} & a_{2,2} & \dots & a_{2,j} \\ \dots & \dots & \dots & \dots \\ a_{i,1} & a_{i,2} & \dots & a_{i,j} \end{bmatrix} \quad (1)$$

$$TP_i = a_{i,i} \quad (2)$$

$$FP_i = \sum_1^i a_{j,i} - TP_i \quad (3)$$

$$FN_i = \sum_1^i a_{i,j} - TP_i \quad (4)$$

$$OA = \frac{\sum_i^i TP_i}{\sum_1^i \sum_1^j a_{i,j}} \quad (5)$$

$$Pr_i = \frac{TP_i}{TP_i + FP_i} \quad (6)$$

$$Re_i = \frac{TP_i}{TP_i + FN_i} \quad (7)$$

$$F_{1i} = 2 \cdot \frac{Pr_i \cdot Re_i}{Pr_i + Re_i} \quad (8)$$

where A represents the confusion matrix (1), TP_i is True Positives (2), FP_i is False Positives (3), FN_i is False Negatives (4), OA is the overall accuracy (5), Pr_i is the precision (6), Re_i is the recall (7), and F_{1i} is the F-measure (8).

4. Results

Two independent classifications were conducted, using two files including 3D points as entry data. They were obtained after a photogrammetric process, and were composed of 14,094,898 points in the case of the RGB cloud (.las file), and 1,374,606 points from the MS cloud (.txt file). Their positional error was estimated through the root-mean-square error (RMSE) between the position of the computed 3D point and the corresponding GCPs, being 2.79 cm for the RGB cloud and 1.67 cm for the MS cloud.

4.1. Bare-ground points classification

After the selection of the training samples, the software was run for the supervised classification of ground and vegetation classes. In this run, all the classification models were analysed (Fig. 4).

Fig. 4 summarizes the statistical data displayed by Class3Dp during the search for the best model. This figure shows the cross-validation values of each model. All methods generated accurate results with a range score between 0.86 (MultiLayer Perceptron outlier) and 1 for the RGB classification and 0.99 and 1 for the MS classification. In the case of RGB classification, the highest mCVs were obtained by Random Forest (0.999), while in MS classification, mCVs equal to 1 were obtained for the Decision Tree and Gradient Boosting models.

Once the results of the models were obtained, it was decided not to perform a fine-tuning of the hyperparameters, due to those high accurate values obtained. Therefore, the RGB point cloud was classified using Random Forest, while the MS point cloud was classified with Gradient Boosting (Fig. 5). When running these models, the features with the highest permutation importance were evaluated, finding that in the RGB

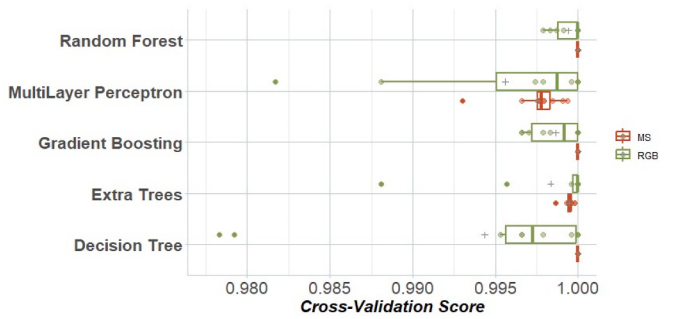


Fig. 4. Box and whiskers plot of cross-validation scores for the five classifiers analysed for ground and vegetation classification in RGB (green) and MS (red) point clouds. Outliers are plotted with circle symbols. An outlier detected in the RGB MultiLayer Perceptron is not represented (0.86).

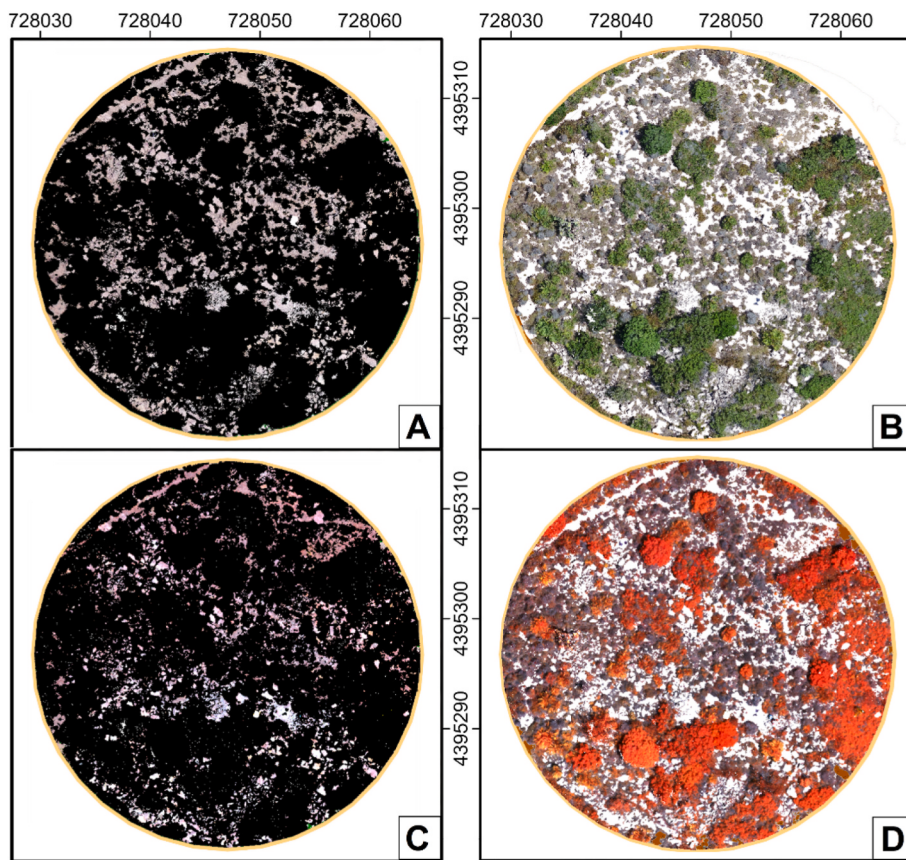


Fig. 5. (A) Zenithal view of the points classified as ground in the RGB point cloud with black background. (B) Points classified as vegetation in the RGB point cloud with white background. (C) False-colour infrared points classified as ground in the MS point cloud with black background. (D) False-colour infrared points classified as vegetation in the MS point cloud with white background.

Table 2

Ground and vegetation classification confusion matrix with precision (Pr), recall (Re), and F-measure (Fm) and overall accuracy (OA) for the different classes. Values indicate the number of points collected for evaluation.

		RGB		MS	
		Classified as			
Truth		Ground	Vegetation	Ground	Vegetation
	Ground	85,852	105	19,169	0
Vegetation	12,540	98,145	1481	7976	
Pr	0.873	0.995	0.928	0.998	
Re	0.811	0.997	0.972	0.996	
Fm	0.841	0.996	0.950	0.997	
OA	0.936		0.948		

classification, there were three features with non-zero permutation importance: NGRDI_mean, SAVI and verticality, which obtained values of 0.03, 0.11 and 0.50, respectively. In contrast, in the MS classification only one variable obtained a value greater than zero, NDVI_mean with a value of 0.47.

Once the point clouds were classified, they were compared with the validation data, obtaining the confusion matrix shown in Table 2.

Analysing in detail the classification of the RGB point cloud, the results from the confusion matrix showed that a total of 85,852 ground points and 98,145 vegetation points were correctly classified from a total of 196,642 points. These numbers give a high OA (0.936), but other statistics need to be analysed in detail due to the imbalance of the classes. On the one hand, focusing on the vegetation class, a score of 0.995 for Pr implies a very high accuracy in the prediction of vegetation points. Another value that is also close to one is obtained for Re (0.997),

where the correctly classified values are compared to incorrect values. Similarly, the Fm obtains a value close to one (0.996), representing the harmonic mean of precision and recall. An adequate Fm is associated with low values of FP and FN, as in this case. These values indicate high correctness in the prediction of vegetation points. On the other hand, in the ground class, we observe equally high statistical values, highlighting a Pr of 0.873 and a Fm of 0.841. Although the values obtained were less remarkable, they still indicate a sound classification, predicting practically all the vegetation points correctly. Regarding the multispectral classification, the addition of the two spectral bands, RedEdge and NIR, has a positive impact on all statistics, slightly improving the OA from 0.936 of the RGB classification to 0.948. These values are more remarkable in the ground class, obtaining values close to one in Pr (0.928), Re (0.972) and Fm (0.950). With the MS point cloud, the vegetation class scores were very similar to those obtained using the RGB point cloud.

4.2. Species classification results

The classification of plant species began with a fine-tuning of the hyperparameters to optimize the accuracy of the models. Class3Dp creates a file with a statistical summary at the end of the hyperparameter fine-tuning. This file stores the cross-validation scores obtained in each of the 10 iterations carried out with each combination of hyperparameters. Table 3 is based on these values. This table shows the summary of the results obtained during the search for hyperparameters in the classification of plant species.

After executing the hyperparameter search, Class3Dp automatically selects the hyperparameters that have obtained the best mCVS and uses them to generate the model that predicts the classified point cloud. After

Table 3

Mean cross-validation score obtained in the hyperparameters fine-tuning for the models: Decision Tree, Extra Trees, Gradient Boosting, Random Forest and MultiLayer Perceptron for the RGB (green colour gradient) and MS (red colour gradient) point clouds. The colour gradient is intensified according to the improvement of the result.

RGB												Multispectral												
Min. number of samples to split an internal node	Decision Tree			Extra Trees			Gradient Boosting			Decision Tree			Extra Trees			Gradient Boosting								
	2	3	5	2	3	5	2	3	5	2	3	5	2	3	5	2	3	5	2	3	5	2	3	5
1	0.633	0.633	0.633	0.636	0.642	0.632	0.738	0.738	0.738	0.715	0.714	0.715	0.681	0.683	0.679	0.830	0.829	0.829	0.830	0.830	0.829	0.830	0.830	0.829
2	0.633	0.633	0.633	0.638	0.639	0.645	0.737	0.738	0.738	0.714	0.714	0.714	0.679	0.681	0.679	0.830	0.830	0.829	0.830	0.830	0.829	0.830	0.830	0.829
5	0.633	0.633	0.633	0.638	0.638	0.642	0.739	0.739	0.739	0.714	0.714	0.714	0.677	0.679	0.682	0.828	0.829	0.827	0.828	0.829	0.827	0.828	0.829	0.827
1	0.669	0.667	0.667	0.706	0.707	0.707	0.770	0.765	0.761	0.761	0.761	0.759	0.759	0.759	0.842	0.842	0.843	0.842	0.843	0.843	0.842	0.843	0.843	0.843
2	0.667	0.668	0.667	0.707	0.708	0.705	0.763	0.765	0.765	0.759	0.759	0.758	0.756	0.757	0.761	0.844	0.843	0.843	0.844	0.843	0.843	0.844	0.843	0.843
5	0.669	0.668	0.667	0.704	0.705	0.706	0.765	0.766	0.764	0.759	0.758	0.760	0.758	0.755	0.758	0.847	0.846	0.847	0.847	0.846	0.847	0.847	0.846	0.847
1	0.701	0.699	0.701	0.779	0.778	0.777	0.734	0.737	0.735	0.774	0.771	0.771	0.824	0.826	0.823	0.787	0.789	0.806	0.787	0.789	0.806	0.787	0.789	0.806
2	0.705	0.701	0.701	0.776	0.776	0.776	0.727	0.730	0.731	0.770	0.768	0.769	0.819	0.819	0.817	0.821	0.819	0.823	0.821	0.819	0.823	0.821	0.819	0.823
5	0.698	0.700	0.703	0.767	0.768	0.768	0.730	0.732	0.732	0.767	0.768	0.770	0.805	0.803	0.804	0.836	0.837	0.836	0.836	0.837	0.836	0.836	0.837	0.836

Random Forest																							
Number of trees in the forest			200			500			200			500											
Number of features to consider for the best split			auto	sqr7	log2																		
Function to measure the quality of a split	Gini	0.656	0.657	0.653	0.653	0.657	0.654	0.693	0.689	0.689	0.694	0.694	0.690	0.690	4								
	Gini	0.676	0.676	0.674	0.677	0.676	0.673	0.718	0.716	0.712	0.717	0.715	0.714	0.714	5								
	Gini	0.694	0.692	0.688	0.693	0.692	0.688	0.739	0.741	0.733	0.739	0.740	0.736	0.736	6								
	Gini	0.704	0.704	0.701	0.704	0.705	0.702	0.758	0.757	0.754	0.759	0.760	0.754	0.754	7								
	Gini	0.715	0.715	0.712	0.714	0.715	0.711	0.773	0.773	0.770	0.775	0.773	0.771	0.771	8								
	Entropy	0.661	0.659	0.662	0.662	0.662	0.662	0.697	0.699	0.695	0.699	0.699	0.697	0.697	4								
	Entropy	0.685	0.682	0.679	0.685	0.684	0.681	0.722	0.722	0.716	0.722	0.720	0.718	0.720	5								
	Entropy	0.697	0.698	0.694	0.698	0.697	0.695	0.745	0.747	0.742	0.747	0.746	0.740	0.740	6								
	Entropy	0.709	0.711	0.706	0.708	0.710	0.707	0.765	0.767	0.764	0.766	0.765	0.762	0.762	7								
	Entropy	0.719	0.720	0.718	0.720	0.721	0.717	0.780	0.779	0.776	0.779	0.779	0.776	0.776	8								

MultiLayer Perceptron																						
Learning rate		Constant			Adaptive			Constant			Adaptive											
Alpha	Optimizer	0.0001	0.05	SGD	Adam	SGD	Adam	SGD	Adam	SGD	Adam	SGD	Adam	SGD	Adam	SGD	Adam					
Activation function for the hidden layer	Tanh	0.413	0.541	0.414	0.553	0.407	0.536	0.413	0.547	0.382	0.583	0.395	0.621	0.385	0.598	0.383	0.628	50,50,50				
	Tanh	0.414	0.531	0.413	0.535	0.413	0.538	0.419	0.549	0.383	0.593	0.382	0.593	0.382	0.600	0.382	0.612	50,100,50				
	Tanh	0.413	0.544	0.416	0.575	0.414	0.550	0.420	0.559	0.378	0.627	0.391	0.632	0.401	0.635	0.394	0.627	100				
	Tanh	0.286	0.546	0.224	0.625	0.255	0.640	0.224	0.619	0.382	0.771	0.382	0.769	0.382	0.768	0.382	0.774	50,50,50				
	RELU	0.255	0.648	0.192	0.617	0.255	0.640	0.286	0.626	0.382	0.774	0.382	0.766	0.382	0.788	0.382	0.776	50,100,50				
	RELU	0.412	0.617	0.412	0.593	0.412	0.582	0.412	0.581	0.382	0.630	0.382	0.666	0.382	0.646	0.382	0.599	100				
	RELU	0.412	0.617	0.412	0.593	0.412	0.582	0.412	0.581	0.382	0.630	0.382	0.666	0.382	0.646	0.382	0.599					
	RELU	0.412	0.617	0.412	0.593	0.412	0.582	0.412	0.581	0.382	0.630	0.382	0.666	0.382	0.646	0.382	0.599					
	RELU	0.412	0.617	0.412	0.593	0.412	0.582	0.412	0.581	0.382	0.630	0.382	0.666	0.382	0.646	0.382	0.599					
	RELU	0.412	0.617	0.412	0.593	0.412	0.582	0.412	0.581	0.382	0.630	0.382	0.666	0.382	0.646	0.382	0.599					

this process, the software generates a CSV file with the summary of the results obtained from the calculated hyperparameter combinations. Table 3 has been generated from this CSV file for the case study. From this table, we can observe that regardless of the model chosen, the MS classification obtains better results than the RGB classification. Regarding the RGB classification, we can observe that the model with the highest mCVs is Extra Trees, parameterized with Maximum depth of the tree equal to None, Minimum number of samples to split an internal node with a value of 2 and Min. number of samples required to be at a leaf node equal to 1, obtaining a mCVs of 0.779. Similar results are achieved using the Gradient Boosting model, parameterizing the Maximum depth of the tree to 10, obtaining mCVs values around 0.76. Regarding the MS classification, the model with the highest mCVs (0.846) is Gradient Boosting using the hyperparameters Maximum

depth of the tree equal to 10, Minimum number of samples to split an internal node with a value of 5 and Minimum number of samples required to be at a leaf node equal to 5. Regardless of the hyperparameters used, the best overall results were reached with the Gradient Boosting model, with a minimum value of 0.787 (Table 3). An aspect that should be highlighted in both classifications, whether the point cloud was RGB or MS, is that not introducing a tree depth limit is counterproductive, since if the depth of the tree is not limited, the mCVs decreases. In this sense, this hyperparameter is the one that most affects the results. In contrast, in the MultiLayer Perceptron method, the hyperparameter that most affects the results is the Optimizer, detecting how the Adam optimizer obtains better results than the SGD optimizer (Table 3).

After creating the model, Class3Dp displays the permutation

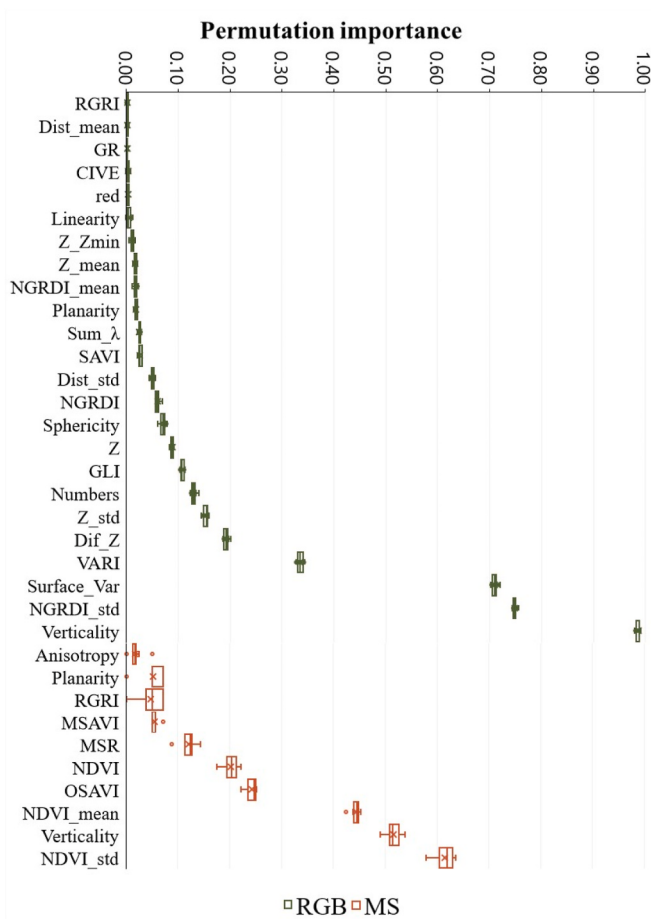


Fig. 6. Permutation feature importance obtained for all features with a value greater than zero for the RGB (green) and MS (red) point cloud classification.

importance obtained for each feature (Fig. 6). We can observe that, as in the previous classification between ground and vegetation, the classification of the RGB point cloud has a greater number of features with permutation importance greater than zero, using in this case, 24 features, while in the MS classification only 10 features obtained a permutation importance greater than zero.

Both in RGB and multispectral classification, the standard deviation of the neighbourhood spectral variable (NGRDI in the case of the RGB cloud and NDVI in the case of the MS cloud) is one of the features with the highest importance, together with verticality. Regarding the 10 features with the highest permutation importance, we find that in the case of the RGB classification there are seven geometric and three spectral features, while in the MS classification, we find seven spectral and three geometric features.

Finally, the point clouds were classified using the models with the highest mCVs: Extra Trees in the case of RGB classification and Gradient Boosting in the case of MS classification (Fig. 7). Once the classified point clouds were obtained, the predicted results were compared with the validation data (Table 4).

Analysing the overall accuracy, we can see how it resembles the mCVs obtained during model fitting. In the case of the RGB point cloud, the results have improved (from 0.779 mCVs obtained in the Extra Trees model to 0.858 OA). In the case of the MS point cloud, the results follow the same trend (from 0.847 mCVs obtained in the Gradient Boosting model to 0.875 OA). In both classifications, the results were similar, with *Anthyllis cytisoides* and *Cistus monspeliensis* being the best classified species. Observing the statistics individually, we can see that most of them are above 0.9, with no notable confusion between the species studied. Based on the recall obtained for *Quercus coccifera* and *Pistacia*

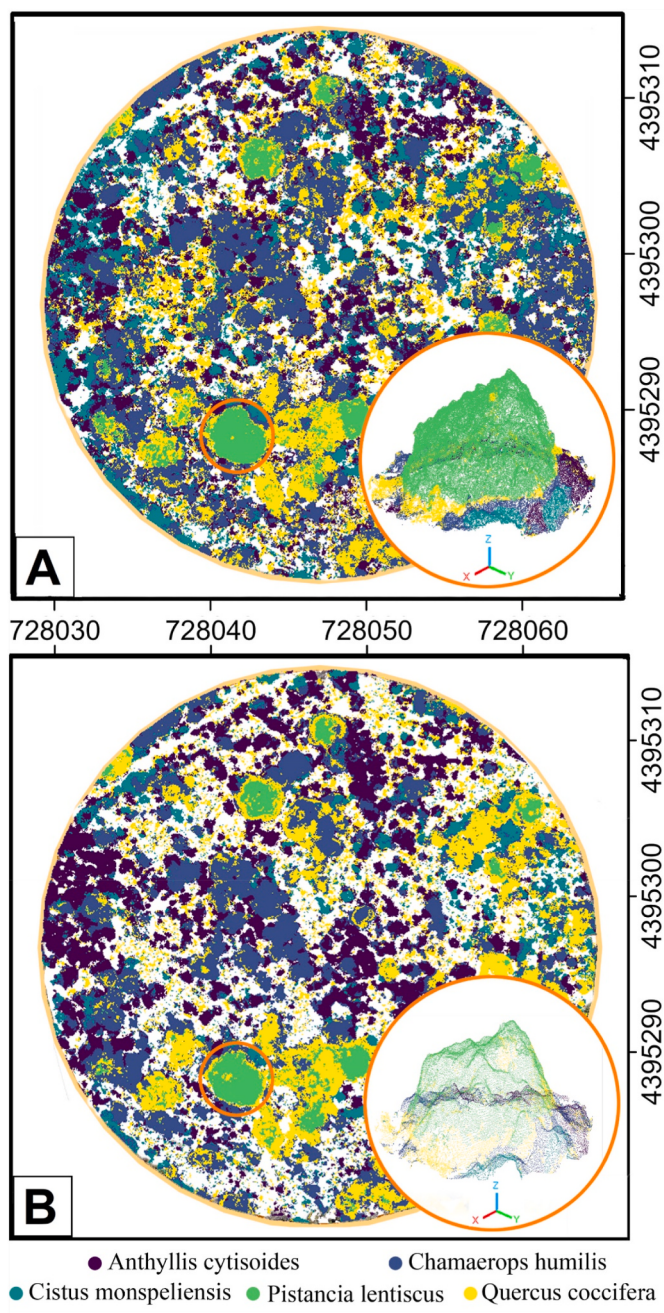


Fig. 7. (A) Zenithal view of the RGB point cloud classified according to classes *Anthyllis cytisoides*, *Chamaerops humilis*, *Cistus monspeliensis*, *Pistacia lentiscus* and *Quercus coccifera*. (B) MS point cloud classified according to the same classes as described previously. Lower right corner of both images, oblique point cloud detail.

lentiscus in both classifications (RGB and MS), we can observe that these classes obtained the most confusion among the species studied.

5. Discussion

The possibility of having a point cloud classified according to plant species allows the availability of ecosystem information that can be essential for describing, understanding, predicting or managing biodiversity (De Cáceres et al., 2015; Guo et al., 2017; Hernandez-Stefanoni et al., 2006). This information can allow technicians to know the representativeness of each species, its location or its dimensions, being useful for specific cases as quantity forest structure and composition

Table 4

Species' confusion matrix obtained from independent validation samples with precision (Pr), recall (Re), F-measure (Fm) and overall accuracy (OA) for the different classes. Values indicate the number of points collected involved in the validation. Column headers are class labels, rows refer to class indices. The green gradient is associated with RGB values, while the red gradient represents MS values.

		RGB				MS					
		Classified as									
		Anthyllis cytisoides	Chamaerops humilis	Cistus monspeliensis	Pistacia lentiscus	Quercus coccifera	Anthyllis cytisoides	Chamaerops humilis	Cistus monspeliensis	Pistacia lentiscus	Quercus coccifera
Truth	1	25,504	39	262	0	6	2,901	0	0	0	0
	2	348	113,396	530	4,161	22,587	43	7,630	20	99	1,123
	3	0	189	33,449	35	20	0	9	2,809	3	0
	4	0	911	0	80,196	4,833	0	38	0	8,513	1,497
	5	3	7,822	272	19,829	122,663	0	405	0	1,569	11,703
Pr		0.986	0.927	0.969	0.769	0.817	0.985	0.944	0.993	0.836	0.817
Re		0.988	0.804	0.993	0.933	0.815	1.000	0.856	0.996	0.996	0.856
Fm		0.987	0.861	0.981	0.843	0.816	0.993	0.898	0.994	0.909	0.836
OA		0.858				0.875					

(Alonso et al., 2018; Molina-Valero et al., 2022), ecological monitoring (Arroyo-Mora et al., 2019), understanding and protecting ecosystems (Mangewa et al., 2019), or making informed decisions regarding conservation (Baena et al., 2018).

During the processing of point clouds for forestry applications, one of the most generalized steps is the normalization of the point cloud heights. This normalization reduces the height to zero-level to perform height measurements of the elements contained in the point cloud without being affected by the different heights of the terrain (Malambo et al., 2018; Nevalainen et al., 2017; Wang et al., 2008). To perform this height normalization, it is necessary to classify the bare-ground points and subsequently interpolate them to generate a surface representing the terrain. As mentioned previously, software such as LAStools (Isenburg, 2014) or Fusion/LDV (McGaughey, 2016) allow us for the classification of bare-ground points using the geometric characteristics of photogrammetric point clouds. Previous studies tested the possibility of using these software tools in the classification of ground points in Mediterranean forests, obtaining an OA of 0.725 in the case of Fusion and 0.733 in the case of LAStools (Zeybek and Şanlıoglu, 2019). Class3Dp, combining geometric, spectral and neighbourhood features, enables the collection of training samples and the classification of RGB and MS point clouds (Fig. 4). In the models analysed, values of mCVs close to one have been obtained. The software has allowed an optimal discrimination between bare ground and vegetation, considering the difficulty of differentiating bare ground from small shrubs and grasses that form a continuous horizontal surface. In the case study, the same areas have been used as training samples for both the RGB and MS point clouds. In each training sample, the RGB point cloud had higher density, while the MS cloud had higher spectral resolution. In the classification of vegetation species, better results were obtained by having higher spectral resolution than point density.

In the classification of species, hyperparameter tuning was performed, in which the software automatically searches for the hyperparameters that obtain the best mCVs in the tuning. This tuning helped to optimize machine learning models, increasing classification accuracy, reducing the time required for training, and avoiding overfitting of the data (Probst and Bischl, 2019). A model search and fine-tuning of each model improved the models by more than 50%, comparing the best and worst values of mCVs obtained in the classification results (Table 3).

The good results obtained in both classifications are noteworthy, bearing in mind the difficulty involved in classifying plant species. This

type of classification deals with problems such as the intraspecific differences of each species at different growth stages (i.e., the changes in shape and loss of green colour of the leaves of *Quercus coccifera*, or the change in the intensity of the green colour of the leaf of *Pistacia lentiscus* as each individual matures) or the interrelation between individuals of different species competing in the same soil space at different heights.

Currently, to the best of the authors' knowledge, there is no free software available to classify point clouds based on their geometric and spectral information. Prior to the release of Class3Dp, there have been previous studies in which point clouds were classified using geometric and spectral features. In 2017, Nevalainen et al. classified four boreal forest tree species using hyperspectral information. In this study, 347 spectral and geometrical features were used to train different machine learning models (k-nearest neighbours, Random Forest, and MultiLayer Perceptron). The last two classifiers obtained 95% of overall accuracy. Tuominen et al. (2018) conducted a more arduous study with a similar methodology. They employed 692 spectral and geometrical features obtained from UAV-DAP point clouds and hyperspectral image mosaics and applied k-nearest neighbours and Random Forest classifiers to classify 26 different tree species in southeastern Finland. The k-nearest neighbours classifier achieved the highest global accuracy, with an accuracy rate of 82%. Sothe et al. (2019) used 68 spectral and geometrical features and a support vector machine classifier to classify 12 major tree species in a subtropical forest by integrating UAV-DAP point cloud and hyperspectral data. In this study, an overall accuracy rate of 72% was achieved. These studies, where no specific software tools were presented, highlight the potential of a software for point cloud supervised classification.

6. Conclusions and future works

We have proposed a software for supervised classification of vegetation species from coloured point clouds. Unlike existing software that allows the classification of point clouds, this software introduces two improvements: the possibility to classify point clouds based on training samples and the addition of spectral features to the classification of UAV-DAP point clouds. In this respect, the automation of the pipeline and the graphical interface of Class3Dp allows users to perform supervised classifications quickly and intuitively. In our tests, we have demonstrated the effectiveness and robustness of the proposed software in different classifications. Class3Dp allows for the classification of both ground and vegetation points, as well as the plant species studied. Hence, Class3Dp can produce a more accurate and precise classification, not only in the classification of plant species but also in any classification of a coloured point cloud. Although focused on plant species classification, this software can be used in a wide range of fields (archaeology, architecture, biodiversity, construction, cultural heritage, forestry, mining, topography ...). Future works will focus on the inclusion of indices obtained from hyperspectral images, since point clouds from images taken with hyperspectral snapshot cameras can be obtained. Class3Dp is a free software that allows all interested users to use it for all kinds of studies where point clouds can be relevant to extract useful information.

Funding

This research has been supported by the grants BES-2017-081920 and PID2020-117808RB-C21 funded by MCIN/AEI/10.13039/501100011033 and by ESF Investing in your future. Funding for open access charge: Universitat Politècnica de València.

Declaration of competing interest

The authors declare that they have no known competing financial interests or personal relationships that could have appeared to influence the work reported in this paper.

Data availability

The software and dataset used are available in the "RiuNet" repository under open access license. Both elements are referenced in the manuscript.

Appendix A. Supplementary data

Supplementary data to this article can be found online at <https://doi.org/10.1016/j.envsoft.2023.105859>.

References

- Agisoft LLC, 2022. Metashape Professional.
- Al-doski, J., Mansor, S.B., Zulhaidi, H., Shafri, M., 2013. Image classification in remote sensing. *J. Environ. Earth Sci.* 3, 141–148.
- Alonso, M., Andersen, H.-E., Morton, D.C., Cook, B.D., 2018. Quantifying boreal forest structure and composition using UAV structure from motion. *Forests* 9, 119.
- Arroyo-Mora, J., Kalacska, M., Inamdar, D., Soffer, R., Lucanus, O., Gorman, J., Naprstek, T., Schaaf, E., Ifimov, G., Elmer, K., Leblanc, G., 2019. Implementation of a UAV-hyperspectral pushbroom imager for ecological monitoring. *Drones* 3, 12. <https://doi.org/10.3390/drones3010012>.
- Atik, M.E., Duran, Z., Seker, D.Z., 2021. Machine learning-based supervised classification of point clouds using multiscale geometric features. *ISPRS Int. J. Geo-Inf.* <https://doi.org/10.3390/ijgi10030187>.
- Baena, S., Boyd, D.S., Moat, J., 2018. UAVs in pursuit of plant conservation—Real world experiences. *Ecol. Inf.* 47, 2–9.
- Barbosa, B.D.S., Ferraz, G.A.S., Gonçalves, L.M., Marin, D.B., Maciel, D.T., Ferraz, P.F.P., Rossi, G., 2019. RGB vegetation indices applied to grass monitoring: a qualitative analysis. *Agron. Res.* 17, 349–357. <https://doi.org/10.15159/AR.19.119>.
- Breiman, L., 2001. Random forests. *Mach. Learn.* 45, 5–32.
- Cabo, C., Ordóñez, C., Sánchez-Lasheras, F., Roca-Pardiñas, J., de Cos-Juez, J., 2019. Multiscale supervised classification of point clouds with urban and forest applications. *Sensors*. <https://doi.org/10.3390/s19204523>.
- Carbonell Rivera, J.P., Ruiz Fernández, L.Á., Estornell Cremades, J., 2023a. Class3Dp.
- Carbonell Rivera, J.P., Torralba Pérez, J., Crespo Peremarch, P., Ruiz Fernández, L.Á., 2023b. RGB and Multispectral Point Clouds of the Sierra Calderona Natural Park. <https://doi.org/10.4995/DATASET/10251/194199>.
- Carbonell-Rivera, J.P., Estornell, J., Ruiz, L.Á., Torralba, J., Crespo-Peremarch, P., 2020. Classification of UAV-based photogrammetric point clouds of riverine species using machine learning algorithms: a case study in the Palancia river, Spain. *Int. Arch. Photogram. Rem. Sens. Spatial Inf. Sci.* 659–666. <https://doi.org/10.5194/ISPRS-ARCHIVES-XLIII-B2-2020-659-2020>.
- Carbonell-Rivera, J.P., Torralba, J., Estornell, J., Ruiz, L.Á., Crespo-Peremarch, P., 2022. Classification of mediterranean shrub species from UAV point clouds. *Rem. Sens.* 14, 199. <https://doi.org/10.3390/rs14101199>.
- Chen, J.M., 1996. Evaluation of vegetation indices and a modified simple ratio for boreal applications. *Can. J. Rem. Sens.* 22, 229–242.
- Cleverdon, C., Keen, M., 1966. Factors Determining the Performance of Indexing Systems, 2.
- Congalton, R., Mead, R., Oderwald, R., Heinen, J., 1981. Analysis of forest classification accuracy. *Remote Sensing Research Report*, 81-1. Nationwide Forestry Applications Program Cooperative. Research Report.
- Costa, L., Nunes, L., Ampatzidis, Y., 2020. A new visible band index (vNDVI) for estimating NDVI values on RGB images utilizing genetic algorithms. *Comput. Electron. Agric.* 172, 105334. <https://doi.org/10.1016/J.COMPAG.2020.105334>.
- De Cáceres, M., Chtry, M., Aguirre, E., Attorre, F., Botta-Dukát, Z., Capelo, J., Czicz, B., Dengler, J., Ewald, J., Faber-Langendoen, D., 2015. A comparative framework for broad-scale plot-based vegetation classification. *Appl. Veg. Sci.* 18, 543–560.
- Demantké, J., Vallet, B., Paparoditis, N., 2012. Streamed vertical rectangle detection in terrestrial laser scans for facade database production. *ISPRS Annals of the Photogrammetry, Remote Sensing and Spatial Information Sciences* I-3, 99–104. <https://doi.org/10.5194/ISPRSANNALS-I-3-99-2012>.
- Deng, A., Wu, Y., Zhang, P., Lu, Z., Li, W., Su, Z., 2022. A weakly supervised framework for real-world point cloud classification. *Comput. Graph.* 102, 78–88.
- Diaz, J.A., Carbonell, R., Virgos, E., Santos, T., Telleria, J.L., 2000. Effects of forest fragmentation on the distribution of the lizard *Psammmodromus algirus*. *Anim. Conserv.* 3, 235–240. <https://doi.org/10.1111/J.1469-1795.2000.TB00108.X>.
- Dong, Y.X., 2014. Review of otsu segmentation algorithm. *Adv. Mater. Res.* 989–994, 1959–1961. <https://doi.org/10.4028/www.scientific.net/AMR.989-994.1959>.
- Ferreira, M.P., Wagner, F.H., Aragão, L.E.O.C., Shimabukuro, Y.E., de Souza Filho, C.R., 2019. Tree species classification in tropical forests using visible to shortwave infrared WorldView-3 images and texture analysis. *ISPRS J. Photogrammetry Remote Sens.* 149, 119–131. <https://doi.org/10.1016/J.ISPRSJPRS.2019.01.019>.
- Fraser, R.H., van der Sluijs, J., Hall, R.J., 2017. Calibrating satellite-based indices of burn severity from UAV-derived metrics of a burned boreal forest in NWT, Canada, 2017. *Rem. Sens.* 9, 279. <https://doi.org/10.3390/RS9030279>, 9, 279.
- Friedman, J.H., 2001. Greedy function approximation: a gradient boosting machine. *Ann. Stat.* 1189–1232.
- Gamon, J.A., Surfus, J.S., 1999. Assessing leaf pigment content and activity with a reflectometer. *New Phytol.* 143, 105–117. <https://doi.org/10.1046/J.1469-8137.1999.00424.X>.
- Gao, S., Bilskie, M.V., Hagen, S.C., 2022. PyVF: a python program for extracting vertical features from LiDAR-DEMs. *Environ. Model. Software* 157, 105503. <https://doi.org/10.1016/j.envsoft.2022.105503>.
- Geurts, P., Ernst, D., Wehenkel, L., 2006. Extremely randomized trees. *Mach. Learn.* 63, 3–42.
- Gitelson, A.A., Kaufman, Y.J., Merzlyak, M.N., 1996. Use of a green channel in remote sensing of global vegetation from EOS-MODIS. *Remote Sens. Environ.* 58, 289–298.
- Gitelson, A.A., Kaufman, Y.J., Stark, R., Rundquist, D., 2002. Novel algorithms for remote estimation of vegetation fraction. *Remote Sens. Environ.* 80, 76–87. [https://doi.org/10.1016/S0034-4257\(01\)00289-9](https://doi.org/10.1016/S0034-4257(01)00289-9).
- Gong, P., Pu, R., Biging, G.S., Larrieu, M.R., 2003. Estimation of forest leaf area index using vegetation indices derived from Hyperion hyperspectral data. *IEEE Trans. Geosci. Rem. Sens.* 41, 1355–1362.
- González, E., Balado, J., Arias, P., Lorenzo, H., 2022. Realistic correction of sky-coloured points in Mobile Laser Scanning point clouds. *Opt. Laser. Technol.* 149, 107807. <https://doi.org/10.1016/J.OPTLASTEC.2021.107807>.
- Guo, X., Coops, N.C., Tompalski, P., Nielsen, S.E., Bater, C.W., Stadt, J.J., 2017. Regional mapping of vegetation structure for biodiversity monitoring using airborne lidar data. *Ecol. Inf.* 38, 50–61.
- Hernandez-Stefanoni, J.L., Pineda, J.B., Valdes-Valadez, G., 2006. Comparing the use of indigenous knowledge with classification and ordination techniques for assessing the species composition and structure of vegetation in a tropical forest. *Environ. Monit. Assess.* 686–702.
- Hinton, G.E., 1990. Connectionist learning procedures. In: *Machine Learning*. Elsevier, Washington, DC, USA., pp. 555–610
- Hooper, D.U., Vitousek, P.M., 1997. The effects of plant composition and diversity on ecosystem processes. *Science* 277, 1302–1305. <https://doi.org/10.1126/science.277.5330.1302>, 1979.
- Huete, A.R., 1988. A soil-adjusted vegetation index (SAVI). *Remote Sens. Environ.* 25, 295–309.
- Huete, A., Justice, C., Van Leeuwen, W., 1999. MODIS Vegetation Index (MOD13), Algorithm Theoretical Basis Document. NASA Goddard Space Flight Center Greenbelt, MD 20771, USA.
- Hunt, E.R., Cavigelli, M., Daughtry, C.S.T., McMurtrey, J.E., Walthall, C.L., 2005. Evaluation of digital photography from model aircraft for remote sensing of crop biomass and nitrogen status. *Precis. Agric.* 6, 359–378.
- Iglhaut, J., Cabo, C., Puliti, S., Piermattei, L., O'Connor, J., Rosette, J., 2019. Structure from motion photogrammetry in forestry: a review. *Current Forestry Reports* 5, 155–168. <https://doi.org/10.1007/S40725-019-00094-3/FIGURES/4>.
- Isenburg, M., 2014. LASTools.
- Ivanova, Y., Kovalev, A., Yakubailik, O., Soukhovolsky, V., 2019. The use of satellite information (MODIS/aqua) for phenological and classification analysis of plant communities, 2019 *Forests* 10, 561. <https://doi.org/10.3390/F10070561>, 10, 561.
- Jordan, C.F., 1969. Derivation of leaf-area index from quality of light on the forest floor. *Ecology* 50, 663–666.
- Kataoka, T., Kaneko, T., Okamoto, H., Hata, S., 2003. Crop growth estimation system using machine vision. In: *Proceedings 2003 IEEE/ASME International Conference on Advanced Intelligent Mechatronics (AIM 2003)*, 2, pp. b1079–b1083. <https://doi.org/10.1109/AIM.2003.1225492>.
- Kaufman, Y.J., Tanre, D., 1992. Atmospherically resistant vegetation index (ARVI) for EOS-MODIS. *IEEE Trans. Geosci. Rem. Sens.* 30, 261–270.
- Kingma, D.P., Ba, J., 2014. Adam: A Method for Stochastic Optimization. *arXiv preprint arXiv:1412.6980*.
- Leberl, F., Irschka, A., Pock, T., Meixner, P., Gruber, M., Scholz, S., Wiechert, A., 2010. Point clouds: lidar versus 3D vision. *Photogramm. Eng. Rem. Sens.* 76, 1123–1134. <https://doi.org/10.14358/PERS.76.10.1123>.
- Lu, B., He, Y., 2017. Species classification using Unmanned Aerial Vehicle (UAV)-acquired high spatial resolution imagery in a heterogeneous grassland. *ISPRS J. Photogrammetry Remot. Sens.* 128, 73–85. <https://doi.org/10.1016/j.isprsjprs.2017.03.011>.
- Malambo, L., Popescu, S.C., Murray, S.C., Putman, E., Pugh, N.A., Horne, D.W., Richardson, G., Sheridan, R., Rooney, W.L., Avant, R., Vidrine, M., McCutchen, B., Baltensperger, D., Bishop, M., 2018. Multitemporal field-based plant height estimation using 3D point clouds generated from small unmanned aerial systems high-resolution imagery. *Int. J. Appl. Earth Obs. Geoinf.* 64, 31–42. <https://doi.org/10.1016/J.JAG.2017.08.014>.
- Mangewa, L.J., Ndakidemi, P.A., Munishi, L.K., 2019. Integrating UAV technology in an ecological monitoring system for community wildlife management areas in Tanzania. *Sustainability* 11, 6116.
- Marselis, S.M., Yebra, M., Jovanovic, T., van Dijk, A.I.J.M., 2016. Deriving comprehensive forest structure information from mobile laser scanning observations using automated point cloud classification. *Environ. Model. Software* 82, 142–151. <https://doi.org/10.1016/j.envsoft.2016.04.025>.
- McGaughey, R., 2016. FUSION/LDV: software for LiDAR data analysis and visualization. United States Department of Agriculture, Forest Service, Pacific Northwest Research Station.
- Meinen, B.U., Robinson, D.T., 2021. Agricultural erosion modelling: evaluating USLE and WEPP field-scale erosion estimates using UAV time-series data. *Environ. Model. Software* 137, 104962. <https://doi.org/10.1016/j.envsoft.2021.104962>.
- Mesas-Carrascosa, F.J., de Castro, A.I., Torres-Sánchez, J., Triviño-Tarradas, P., Jiménez-Brenes, F.M., García-Ferrer, A., López-Granados, F., 2020. Classification of 3D point clouds using color vegetation indices for precision viticulture and digitizing applications. *Rem. Sens.* 12, 317.
- Molina-Valero, J.A., Martínez-Calvo, A., Ginzo Villamayor, M.J., Novo Pérez, M.A., Álvarez-González, J.G., Montes, F., Pérez-Cruzado, C., 2022. Operationalizing the

- use of TLS in forest inventories: the R package FORTLS. Environ. Model. Software 150, 105337. <https://doi.org/10.1016/j.envsoft.2022.105337>.
- Nair, V., Hinton, G.E., 2010. Rectified linear units improve restricted Boltzmann machines. In: Proceedings of the 27th International Conference on Machine Learning (ICML-10), pp. 807–814.
- Nevalainen, O., Honkavaara, E., Tuominen, S., Viljanen, N., Hakala, T., Yu, X., Hyppä, J., Saari, H., Pöölön, I., Imai, N., Tommaselli, A., 2017. Individual tree detection and classification with UAV-based photogrammetric point clouds and hyperspectral imaging. Rem. Sens. 9, 185. <https://doi.org/10.3390/rs9030185>.
- Ojala, M., Garriga, G.C., 2010. Permutation tests for studying classifier performance. J. Mach. Learn. Res. 11, 1833–1863.
- Pedregosa, F., Varoquaux, G., Gramfort, A., Michel, V., Thirion, B., Grisel, O., Blondel, M., Prettenhofer, P., Weiss, R., Dubourg, V., 2011. Scikit-learn: machine learning in Python. J. Mach. Learn. Res. 12, 2825–2830.
- Probst, P., Bischl, B., 2019. Tunability: importance of hyperparameters of machine learning algorithms. J. Mach. Learn. Res. 20, 1–32.
- Qi, J., Chehbouni, A., Huete, A.R., Kerr, Y.H., Sorooshian, S., 1994. A modified soil adjusted vegetation index. Remote Sens. Environ. 48, 119–126.
- Ray, T.W., Farr, T.G., Blom, R.G., Crippen, R.E., 1993. Monitoring Land Use and Degradation Using Satellite and Airborne Data.
- Richardson, A.J., Wiegand, C.L., 1977. Distinguishing vegetation from soil background information. Photogramm. Eng. Rem. Sens. 43, 1541–1552.
- Ripley, B.D., 1996. Pattern Recognition and Neural Networks. Cambridge University Press. <https://doi.org/10.1017/CBO9780511812651>.
- Rondeau, G., Steven, M., Baret, F., 1996. Optimization of soil-adjusted vegetation indices. Remote Sens. Environ. 55, 95–107.
- Roujean, J.-L., Breon, F.-M., 1995. Estimating PAR absorbed by vegetation from bidirectional reflectance measurements. Remote Sens. Environ. 51, 375–384.
- Rouse, J.W., Haas, R.H., Schell, J.A., Deering, D.W., Harlan, J.C., 1974. Monitoring the Vernal Advancement and Retrogradation (Green Wave Effect) of Natural Vegetation, p. 371. NASA/GSFC Type III Final Report, Greenbelt, Md.
- Rusu, R.B., 2009. Semantic 3D Object Maps for Everyday Manipulation in Human Living Environments. Munich.
- Sathya, R., Abraham, A., 2013. Comparison of supervised and unsupervised learning algorithms for pattern classification. Int. J. Adv. Res. Artif. Intell. 2, 34–38. <https://doi.org/10.14569/IJARAI.2013.020206>.
- Shimada, S., Matsumoto, J., Sekiyama, A., Aosier, B., Yokohana, M., 2012. A new spectral index to detect Poaceae grass abundance in Mongolian grasslands. Adv. Space Res. 50, 1266–1273. <https://doi.org/10.1016/J.ASR.2012.07.001>.
- Sothe, C., Dalponte, M., Almeida, C.M. de, Schimalski, M.B., Lima, C.L., Liesenberg, V., Miyoshi, G.T., Tommaselli, A.M.G., 2019. Tree species classification in a highly diverse subtropical forest integrating UAV-based photogrammetric point cloud and hyperspectral data. Rem. Sens. 11, 1338. <https://doi.org/10.3390/rs11111338>.
- Stricker, R., Müller, S., Gross, H.-M., 2014. Non-contact video-based pulse rate measurement on a mobile service robot. In: The 23rd IEEE International Symposium on Robot and Human Interactive Communication. IEEE, pp. 1056–1062.
- Tucker, C.J., 1979. Red and photographic infrared linear combinations for monitoring vegetation. Remote Sens. Environ. 8, 127–150.
- Tuominen, S., Näsi, R., Honkavaara, E., Balazs, A., Hakala, T., Viljanen, N., Pöölön, I., Saari, H., Ojanen, H., 2018. Assessment of classifiers and remote sensing features of hyperspectral imagery and stereo-photogrammetric point clouds for recognition of tree species in a forest area of high species diversity. Rem. Sens. 10, 714. <https://doi.org/10.3390/rs10050714>.
- Ullman, S., 1979. The interpretation of structure from motion. In: Proceedings of the Royal Society of London. Series B, Containing Papers of a Biological Character, 203. Royal Society (Great Britain), pp. 405–426. <https://doi.org/10.1098/rspb.1979.0006>.
- Van Rijsbergen, C.J., 1979. Information retrieval. J. Am. Soc. Inf. Sci. 30, 374–375. <https://doi.org/10.1002/asi.4630300621>.
- Vangi, E., D'amicco, G., Francini, S., Giannetti, F., Lasserre, B., Marchetti, M., Chirici, G., 2021. The new hyperspectral satellite PRISMA: imagery for forest types discrimination, 2021 Sensors 21, 1182. <https://doi.org/10.3390/S21041182>, 21, 1182.
- Wallace, L., Lucieer, A., Malenovský, Z., Turner, D., Vopěnka, P., 2016. Assessment of forest structure using two UAV techniques: a comparison of airborne laser scanning and structure from motion (SfM) point clouds. Forests 7, 62. <https://doi.org/10.3390/f7030062>.
- Wang, Y., Weinacker, H., Koch, B., 2008. A lidar point cloud based procedure for vertical canopy structure analysis and 3D single tree modelling in forest, 2008 Sensors 8, 3938–3951. <https://doi.org/10.3390/S8063938>, 8, 3938–3951.
- Wang, D., Wan, B., Qiu, P., Su, Y., Guo, Q., Wang, R., Sun, F., Wu, X., 2018. Evaluating the performance of sentinel-2, Landsat 8 and pléiades-1 in mapping mangrove extent and species. Rem. Sens. 10, 1468. <https://doi.org/10.3390/rs10091468>.
- West, K.F., Webb, B.N., Lersch, J.R., Pothier, S., Triscari, J.M., Iverson, A.E., 2004. Context-driven automated target detection in 3D data 133–143. <https://doi.org/10.1117/12.5425365426> <https://doi.org/10.1117/12.5425365426>
- Yancho, J.M.M., Coops, N.C., Tompaliski, P., Goodbody, T.R.H., Plowright, A., 2019. Fine-Scale spatial and spectral clustering of UAV-acquired digital aerial photogrammetric (DAP) point clouds for individual tree crown detection and segmentation. IEEE J. Sel. Top. Appl. Earth Obs. Rem. Sens. 12, 4131–4148. <https://doi.org/10.1109/JSTARS.2019.2942811>.
- Zeybek, M., Şanlıoglu, İ., 2019. Point cloud filtering on UAV based point cloud. Measurement 133, 99–111.